11

Influence of deformation on optical and optoelectronic properties of quasi-2D van der waals heterostructures based on borophene

© M.M. Slepchenkov¹, D.A. Kolosov¹, O.E. Glukhova^{1,2}

¹ Saratov National Research State University, Saratov, Russia

² I.M. Sechenov First Moscow State Medical University, Moscow, Russia

e-mail: slepchenkovm@mail.ru

Received January 13, 2025 Revised January 20, 2025 Accepted April 07, 2025

In this paper, *ab initio* methods are used to perform a predictive analysis of the effect of tensile/compressive strain on the optical and optoelectronic properties of van der Waals quasi-2D heterostructures formed by a buckled triangular borophene and graphene-like gallium nitride GaN and zinc oxide ZnO. The cases of strain leading to the appearance of an energy gap in the electronic structure of the studied van der Waals heterostructures are considered in detail: uniaxial compression by 14% and biaxial compression by 4% in the case of the borophene/GaN heterostructure and uniaxial tension by 10% and biaxial compression by 6% in the case of the borophene/ZnO heterostructure. It is shown that under uniaxial deformations, the absorption spectra of both heterostructures change most noticeably in the IR range, demonstrating an increase in the absorption coefficient by several times compared to its values in the absence of deformations. The borophene/GaN heterostructure is characterized by the highest absorption value in the IR range under uniaxial compression by 14%. In the case of biaxial deformations, the borophene/GaN heterostructure is also characterized by an increase in the absorption coefficient in the IR range. For the borophene/ZnO heterostructure, in addition to an increase in absorption in the IR range, an increase in the absorption peak in the visible radiation range under biaxial compression by 6% was found. It is shown that axial tensile/compressive deformation causes an increase in photocurrent generation in the studied heterostructures in the IR and visible radiation ranges due to an increase in their absorption coefficient in the specified wavelength ranges.

Keywords: borophene heterostructures, axial tension/compression, density functional theory, absorption spectrum, photocurrent.

DOI: 10.61011/EOS.2025.05.61640.33-25

1. Introduction

After the discovery of graphene [1], there was a noticeable increase in interest in the experimental production and study of two-dimensional (2D) materials [2]. Compared to their bulk counterparts, 2D materials have a larger surface area and higher reactivity, which, combined with the effect of quantum confinement, leads to their unique physical and chemical properties [2]. After graphene studies focused on other 2D materials such as hexagonal boron nitride (h-BN) [3], black phosphorus [4], silicene [5], stanene [6], germanene [7], and transition metal dichalcogenides [8]. Currently, the family of 2D materials continues to be replenished with new members [9], however, only a small part of them are monoelement. The 2D allotropic form of boron, called borophene, stands out among the most interesting monoelement materials [10]. This material has unique elastic, electronic, optical, thermal, and transport properties [11–14], which indicates promising prospects for its use in supercapacitors, energy storage devices, sensors, medical equipment, and optoelectronics [15]. boron is known to have many allotropic modifications. A similar polymorphism is inherent in borophene. The existence of various atomic configurations of 2D boron

nanostructures was predicted using ab initio methods [16]. There are other varieties of 2D boron sheets with hexagonal holes [19], including α -sheet, β -sheet, γ -sheet in addition to sheets with hexagonal and triangular lattices [17], as well as corrugated sheets with triangular lattices [18]. Experimentally, various allotropic forms of borophene can be obtained by atomic layer deposition on metal substrates [2]0. Currently, such configurations of borophene as corrugated with triangular lattice, hexagonal, β 12 and χ^3 are successfully synthesized [14]. According to the results of ab initio calculations, corrugated borophene with a triangular crystal lattice has the highest energy stability [21]. In addition, this allotropic modification of borophene is a strongly anisotropic metal with a high Young's modulus along its armchair direction, exceeding the Young's modulus of graphene [22], and is characterized by a noticeable anisotropy of thermal conductivity [23]. Due to the polymorphism inherent in borophene, it has a good ability to form heterostructures (vertical or lateral) with various 2D materials [24]. Borophene-graphene vertical heterostructures [25–27] were the first to be experimentally implemented, which demonstrated good structural stability. Similar heterostructures are already being used to create a humidity sensor that has shown a sensitivity about 700

28* 435

times higher than that of ordinary graphene and 27 times higher than that of individual borophene [26]. Vertical 2D heterostructures of borophene-MoS₂ are considered as a promising material for the development of gas sensors [28] and humidity sensors with high sensitivity and fast response [29]. The *ab initio* methods predict the creation of vertical heterostructures borophene/g-C₂N [30], borophene/MX₂ (M=Mo, W and X=S,Se) [31] and borophene/InSe [32], which are promising candidates for the implementation of a metal-semiconductor contact with a Schottky barrier.

Borophene van der Waals quasi-2D heterostructures of two types are considered in this paper —borophene/GaN and borophene/ZnO, which we previously predicted using the *ab initio* methods [33]. For their construction, corrugated borophene with a triangular lattice and graphene-like layers of GaN and ZnO were used. The aim of the study is to identify patterns of the influence of stretching/compression deformation on the optical and optoelectronic properties of these heterostructures.

2. Research methods

Calculations of the studied heterostructures were carried out within the framework of the formalism of density functional theory (DFT) in the SIESTA software package [34] using the basic set of polarization functions DZP and the exchange-correlation functional GGA (generalized gradient approximation) formulated by Purdue, Burke and Ernzerhof (PBE) [35]. The presence of van der Waals forces between the layers of the heterostructure was taken into account by introducing the Grimm dispersion corrections [36]. The equilibrium configuration of super-cells of heterostructures was found by minimizing the total energy of the electronic system using the Broyden-Poulay algorithm [37]. relaxation of the structure was carried out until the forces acting on each atom became less than 0.025 eV/Å. In order to exclude the influence of the layers of the heterostructure on each other in a non-periodic direction, the vacuum gap was chosen to be 20,AA. The kinetic energy of the cutoff in the calculations was 150 Ry. The division of the Brillouin zone was carried out according to the Monkhorst-Pack scheme [38] with a grid $12 \times 6 \times 1$ of k-points.

The maximum value of the photocurrent is calculated using the formula

$$I_{\text{max}} = e \int_{0}^{\omega_2} \frac{A(\omega) Power_{\text{solar}}(\omega)}{h\nu} d\omega, \qquad (1)$$

where e is electron charge; $A(\omega)$ is the absorption coefficient; $Power_{solar}(\omega)$ is solar radiation power; $h\nu$ is the solar radiation quantum energy.

The absorption coefficient is calculated in the framework of the unsteady perturbation theory of the first order [39]:

$$A(\omega) = \frac{\omega}{cn(\omega)} \, \varepsilon_2(\omega), \tag{2}$$

where $\varepsilon_2(\omega)$ is the imaginary part of the complex dielectric constant, $n(\omega)$ is the refractive index, c is the speed of light, ω is the frequency of electromagnetic radiation. The imaginary part of the dielectric constant $\varepsilon_2(\omega)$ is determined by the formula of the form

$$\varepsilon_{2}(\omega) = \frac{e^{2}}{\pi m^{2} \omega^{2}} \sum_{\nu,c} \int_{BZ} d\vec{k} |\langle |\psi_{ck}| \hat{\mathbf{e}}, \mathbf{p} |\psi_{\nu k} \rangle|^{2}$$
$$\times \delta(E_{c}(k) - E_{\nu}(k) - \hbar \omega), \tag{3}$$

where summation is performed for each pair of states of the valence (occupied) band and the conduction band (unoccupied), and integration is performed for all k-points in the Brillouin zone, the indices c and v pertain to electronic states in the conduction band and valence band, respectively, $E_{(c,\nu)}(k)$ and $\psi_{(c,\nu),k}$ are the energies and eigenfunctions of these states. The matrix element of the electronic dipole transition lies between the occupied and unoccupied states, where $\hat{\mathbf{e}}$ is the polarization vector, and **P** is the momentum operator. The optical parameters of the van der Waals heterostructures studied were calculated for two different directions of light polarization (vector E parallel to the axis X and parallel to the axis Y) in the wavelength range of $0.28 - 2 \mu m$. Optical characteristics of the studied heterostructures were calculated with the division of the Brillouin zone with a size of a grid of kpoints of $960 \times 480 \times 1$.

Atomistic models of borophene van der Waals heterostructures under compression and tension deformations

A detailed description of the process of obtaining supercells of borophene/GaN and borophene/ZnO heterostructures is contained in the work [33]. Fig. 1 shows their equilibrium configurations. Translation vectors of the borophene super-cell heterostructure/GaN — $L_x = 3.35 \,\text{Å}$ and $L_y = 6.10 \,\text{Å}$; translation vectors of the super-cell of the borophene/ZnO heterostructure— $L_x = 3.28 \,\text{Å}$ and $L_y = 5.83 \,\text{Å}$. The distance between the borophene and GaN layers along the axis Z was 2.91 Å, the distance between the borophene and ZnO layers was 2.51 Å.

Based on the results of previous studies of the electronic structure of borophene/GaN and borophene/ZnO [33] heterostructures, it was found that they have a gap-free band structure, which is attributable to the decisive contribution of corrugated borophene with a triangular lattice to the formation of the conduction band. It is known that the effective use of van der Waals heterostructures in photovoltaics devices, in particular for solar cells, requires to ensure that they have an energy gap between the valence band and the conduction band. Deformation is one of the possible ways to open an energy gap in the band structure of a nanomaterial. In the framework of our previous study, the van der Waals heterostructures of borophene/GaN and

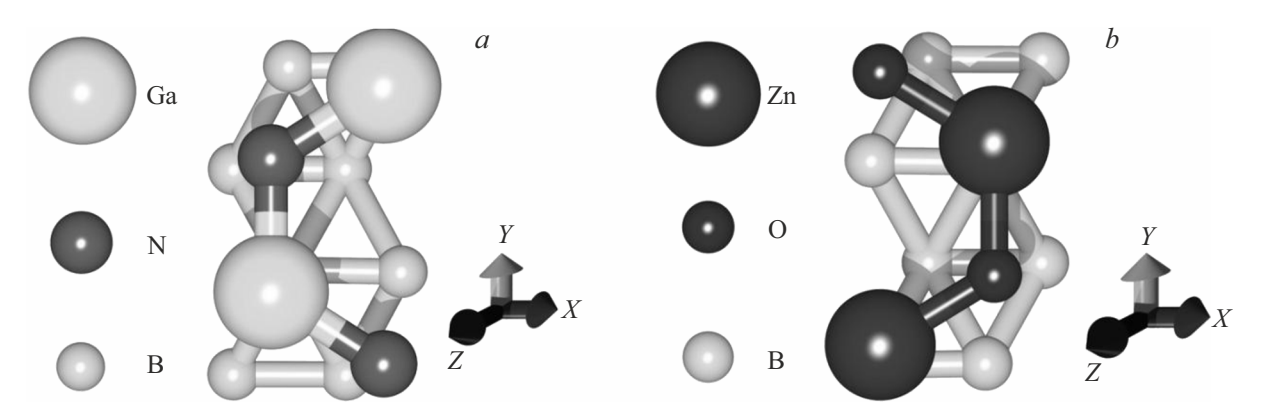


Figure 1. Super-cells of borophene van der Waals heterostructures: (a) borophene/GaN, (b) borophene/ZnO.

borophene/ZnO were subjected to uniaxial and biaxial compression/stretching deformations [40]. We considered the cases of uniaxial compression and stretching deformation along the axis Y (along the zigzag edge of the borophene sheet) by 1-14% and biaxial compression and stretching deformation along the axes X (across the zigzag edge of the borophene sheet) and Y by 1-10%. Based on the results of numerical experiments, it was found that the borophene/GaN heterostructure has an energy gap in cases of uniaxial compression by 14% (0.028 eV) and biaxial compression by 4% (0.018 eV), while the borophene/ZnO heterostructure has an energy gap in cases of uniaxial stretching at 10% (0.063 eV) and biaxial compression at 6% (0.012 eV). Moreover, in order to open the gap, it is necessary to ensure the presence of a zero density of electronic states (DOS) near the Fermi level in the DOS distributions of electronic orbitals and borophene It was the deformation cases and GaN/ZnO atoms. mentioned above that we selected to analyze the optical and optoelectronic properties of deformed van der Waals heterostructures borophene/GaN and borophene/ZnO.

4. Optical and optoelectronic properties of borophene van der Waals heterostructures under compression and stretching deformations

For the studied van der Waals heterostructures, the absorption and photocurrent spectra were calculated in the electromagnetic radiation wavelength range of $0.28-2\,\mu\mathrm{m}$. The calculated absorption spectra for the undeformed and deformed borophene/GaN heterostructure are shown in Fig. 2. The absorption coefficient was numerically estimated for two cases of polarization of electromagnetic radiation: along the axis X (across the zigzag edge of the borophene sheet) and along the axis Y (along the zigzag edge of the borophene sheet). It can be seen from the graphs in Fig. 2, a that the undeformed borophene/GaN heterostructure is characterized by anisotropy of the absorption coefficient. As shown in our previous work in Ref. [41], the observed

anisotropy is explained by the fact that when light is polarized along the axis X, the GaN layer makes a decisive contribution to the optical properties of the borophene/GaN heterostructure, and when light is polarized along the axis Y borophene makes a decisive contribution to the optical properties of the borophene/GaN heterostructure. In both cases of polarization, the absorption peak falls on the region of average UV radiation, but its value is 3 times higher when the light is polarized along the axis Y than when it is polarized along the axis X. Fig. 2, b and 2, cclearly show that both uniaxial and biaxial compressions make significant changes in the absorption spectrum of the borophene/GaN heterostructure, which is primarily attributable to the appearance of an energy gap in its band structure. Uniaxial compression deformation by 14% (Fig. 2, b) caused an increase in the height of the absorption peak in the IR range by 3.5 times with light polarization along the axis X (from 4.5% to 15.8%) and 13 times when the light is polarized along the axis Y (from 1 to 13.2%). The absorption peak shifts in the UV range along the wavelength scale from the mid-UV region to the near-UV region while maintaining its height for the case of light polarization along the axis X and decreases in height by 3.5 times, but remains within the mid-UV region in the case of light polarization along the axes Y. Finally, the peak present in the undeformed heterostructure in the visible range at a wavelength of $0.75 \,\mu\mathrm{m}$ for the case of polarization of light along the axis X after deformation shifts towards the UV range, occupying a wavelength of $0.48 \mu m$ and losing at the same time less than 1% of the height. In case of a biaxial compression by 4% the pattern of changes in the absorption spectrum of the borophene/GaN heterostructure is not as radical as in the case of uniaxial deformation described above, however, it also affects the UV, visible and IR ranges of electromagnetic radiation. A decrease in the height of the absorption peak is observed in the UV range from 6.4% to 3.6% for light polarized along the axis X, and from 18.2 to 12.8% for light polarized along the axis Y. In the IR range, on the contrary, the absorption peak increases for both cases of light polarization: from 4.5 to 6% for polarization along the axis X, from 1 to 2% for

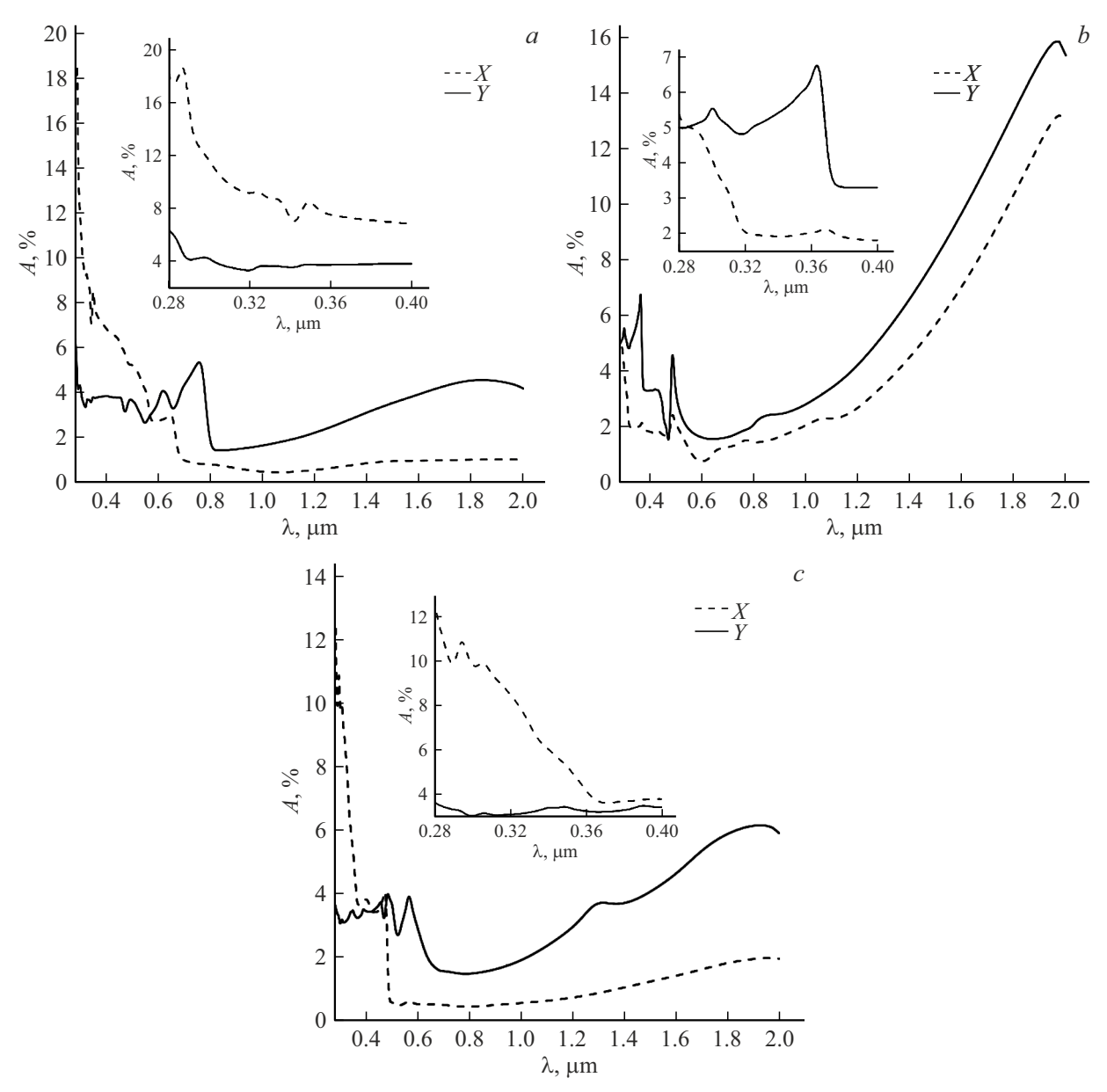


Figure 2. Optical absorption coefficient of the van der Waals borophene/GaN heterostructure when light is polarized along the axes X and Y: (a) in the absence of deformation; (b) with uniaxial compression by 14%; (c) with biaxial compression by 4%. The inserts to the figures show fragments of absorption spectra in the UV wavelength range.

polarization along the axis Y. In the visible range, when light is polarized along the axis of X, the absorption peak splits into two peaks with heights of $\sim 3.8\,\%$ (wavelengths $0.56\,\mu\mathrm{m}$ and $0.45\,\mu\mathrm{m}$), which is $1.5\,\%$ lower than the peak height of the undeformed heterostructure. In general, it can be noted that when light is polarized along the axis Y, uniaxial deformation has a stronger effect on quantitative changes in the absorption coefficient of the borophene/GaN heterostructure.

The reason for the observed differences between the directions of light polarization are the features of the atomic structure of a 2D borophene sheet with a triangular crystal lattice. Let us consider them using the example of an

expanded fragment of the borophene/GaN heterostructure consisting of five super-cells shown in Fig. 1, a. The constructed fragment is shown in Fig. 3 in two projections: the front view (Fig. 3, a) and the side view (Fig. 3, b). It can be seen that boron atoms form zigzag chains with multiple cross-links along the axis Y that provide high resistance to compression deformation acting in the direction of the same axis, while the atoms line up along straight lines in the direction of the axis X.

Let us now discuss the effect of deformation on the absorption spectra of the borophene/ZnO heterostructure, shown in Fig. 4. It can be seen from Fig. 4, a that the undeformed heterostructure is also characterized by anisotropy

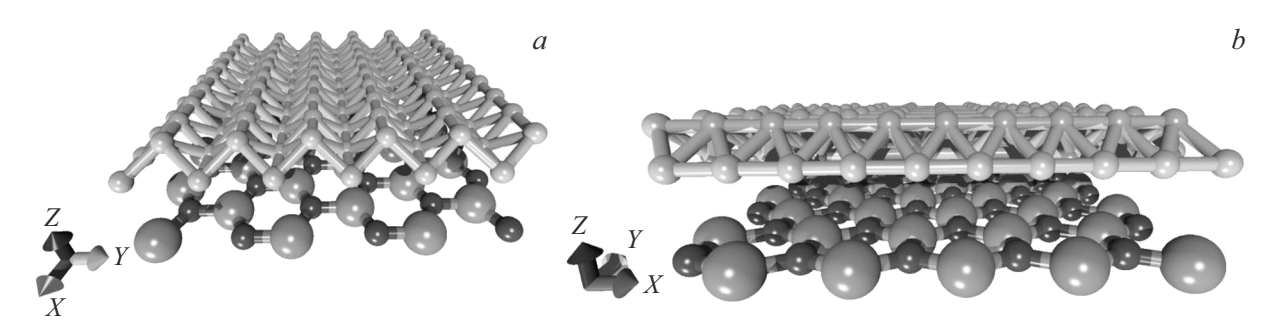


Figure 3. Extended fragment of the borophene/GaN heterostructure, consisting of five super-cells: (a) front view; (b) side view.

of the absorption coefficient when choosing the direction of light polarization, as well as for the borophene/GaN heterostructure. As was shown in our previous paper in Ref. [41], ZnO makes the main contribution to the formation of spectral absorption profiles in the direction of the axis X in the UV and visible ranges and borophene makes the main contribution in the direction of the axis Y, while the synergistic effect of the combination of borophene and ZnO in the composition of the layered structure is also evident in the IR region. In case of uniaxial stretching by 10,%, the greatest changes occur in the IR range (Fig. 4, b): the absorption maximum increases by 2 times in the case of light polarization along the axis X and by 5 times in the case of light polarization along the axis Y. In the latter case, attention is drawn to the appearance of a characteristic peak of maximum intensity at a wavelength of $1.35 \mu m$, which is attributable to the above-mentioned synergistic effect of the interaction of borophene and ZnO in the heterostructure, manifested as an increasing region of characteristics of the real and imaginary parts of the complex dielectric constant in the IR range [41]. The absorption maximum in the near-UV region decreases from 3.7 to 3% in the UV range for light polarized along the axis X, and increases from 8.4 to 11.8% for light polarized along the axis Y. An increase in the absorption maximum by less than 1% is observed in the visible range, and a shift of the wavelength towards the UV range when light is polarized along the axis X, as well as a 3-fold increase when light is polarized along the axis Y. The difference between the directions of light polarization can be explained by the fact that the optical properties of ZnO are significantly manifested in the case of light polarization along the axis X and borophene properties are manifested in the case of the axis Y. Biaxial compression by 6% leads to an increase in the absorption maximum in all three considered ranges of electromagnetic radiation when light is polarized along the axis X: by 1% in the UV range, by 3% (almost twice) in the visible range, and by 2% (almost twice) in the IR range. When the light is polarized along the axis Y, there are no noticeable qualitative changes in the absorption spectrum profile. Quantitative changes in the values of the absorption maximum are observed in the UV range (decrease from 8.4 to 6.2%) and the IR range (increase by 0.2%). In the case of uniaxial tensile

deformation, it can be noted that the optical properties of the borophene/ZnO heterostructure are more sensitive when light is polarized along the axis Y, which, as in the case of the borophene/GaN heterostructure, is explained by the geometric features of the 2D borophene sheet in this direction (the formation of zigzag chains with multiple cross-links). These geometric features can be seen from Fig. 5, where two projections show an expanded fragment of the borophene/ZnO heterostructure consisting of five supercells shown in Fig. 2, a.

Based on the obtained absorption spectra and solar radiation spectra on the Earth's surface (AM1.5) and outside the Earth's atmosphere (AM0), the photocurrent spectra were calculated for the studied van der Waals heterostructures. The solar radiation spectra of AMO and AM1.5 were taken from the website of *National Renewable* Energy Laboratory [42], which shows solar spectra in the wavelength range of $0.28-2\,\mu\text{m}$. The calculated photocurrent spectra of the undeformed and deformed van der Waals heterostructure of borophene/GaN are shown in Fig. 6. The values of the photocurrent are given for a surface area equal to 1 cm^2 . As can be seen from Fig. 6, a, the highest intensity of the integral magnitude of the photocurrent is observed in the region of visible and UV radiation. A decrease in the magnitude of the integral photocurrent is observed starting from a wavelength of $0.8 \,\mu\mathrm{m}$ (IR range), attributable, firstly, to the low absorption coefficient of heterostructures in this range, and secondly, to the lower solar radiation power (the maximum is at a wavelength of $550 \mu m$). An increase in the maximum integral photocurrent in the IR range is observed in case of both uniaxial (Fig. 6, b) and biaxial (Fig. 6, c) compression deformation, and what is more, a threefold increase of the photocurrent peak takes place at a wavelength of $\sim 2 \,\mu \text{m}$ in case of uniaxial compression by 14% compared with an undeformed structure (Fig. 6, a). At the same time, the characteristic peaks in the visible range are preserved for both cases of deformation.

Fig. 7 shows the photocurrent spectra of the undeformed and deformed van der Waals heterostructure of borophene/ZnO. In the absence of deformation, patterns of changes in the absorption coefficient can be observed (Fig. 7, a), similar to the case of the undeformed borophene/GaN heterostructure (Fig. 6, a). Uniaxial stretch-

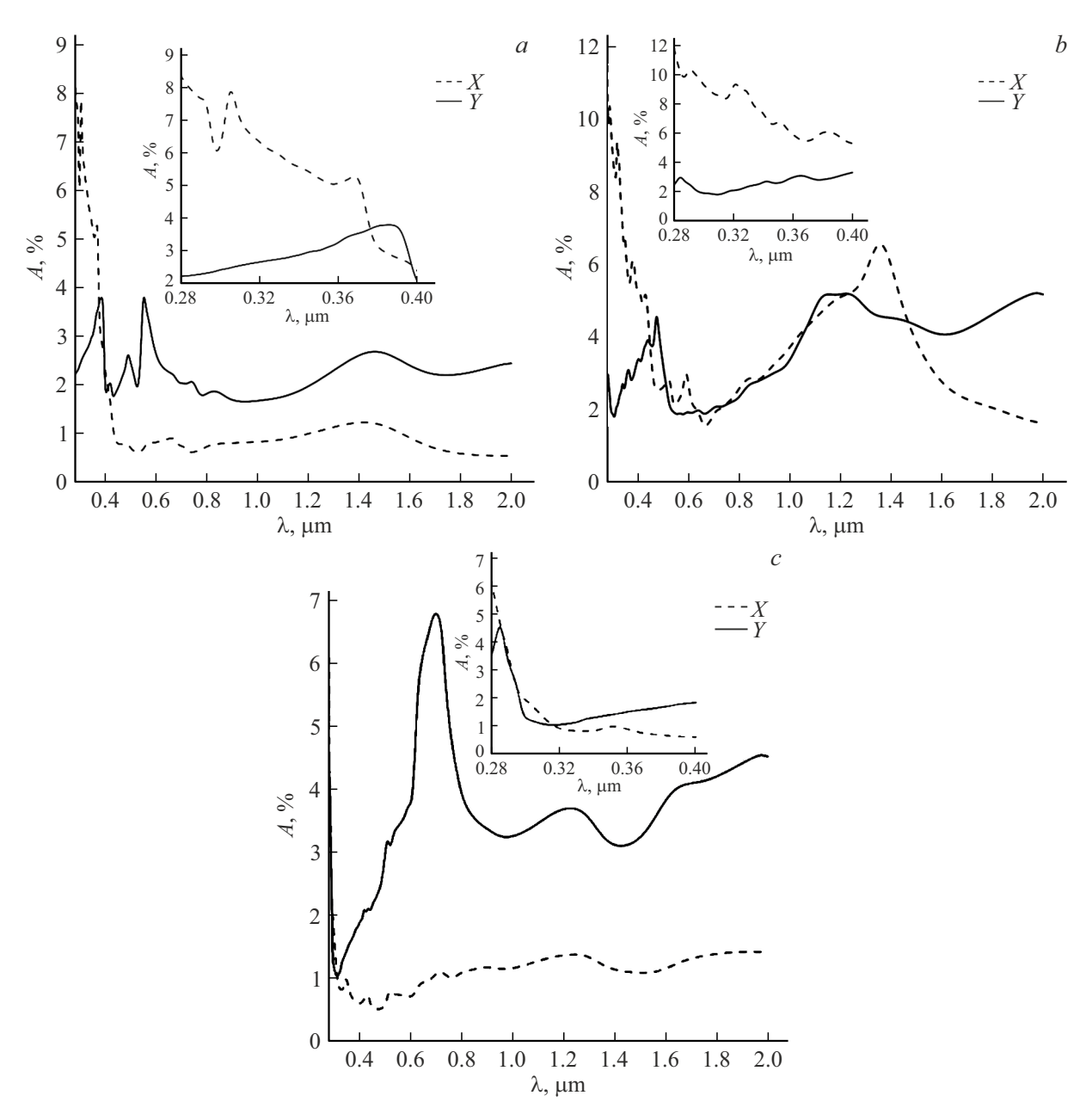


Figure 4. Optical absorption coefficient of the van der Waals borophene/ZnO heterostructure when light is polarized along the axes X and Y: (a) in the absence of deformation; (b) in case of uniaxial tension by 10%; (with) in case of biaxial compression by 6%. The inserts to the figures show fragments of absorption spectra in the UV wavelength range.

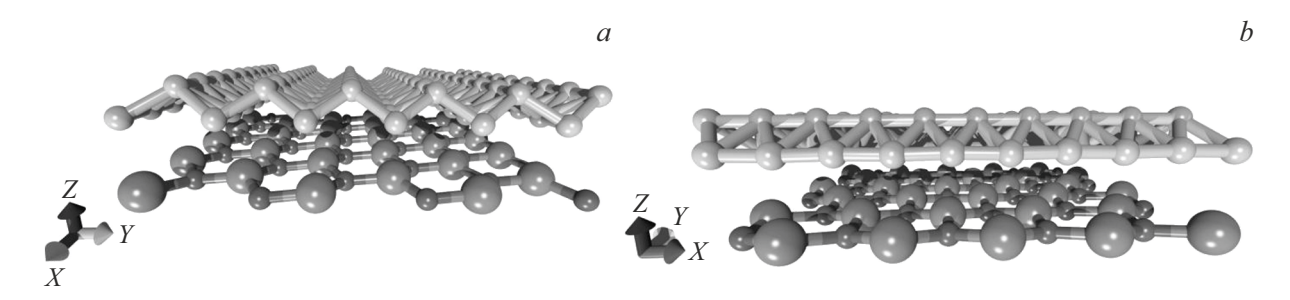


Figure 5. Extended fragment of the borophene/ZnO heterostructure, consisting of five super-cells: (a) front view; (b) side view.

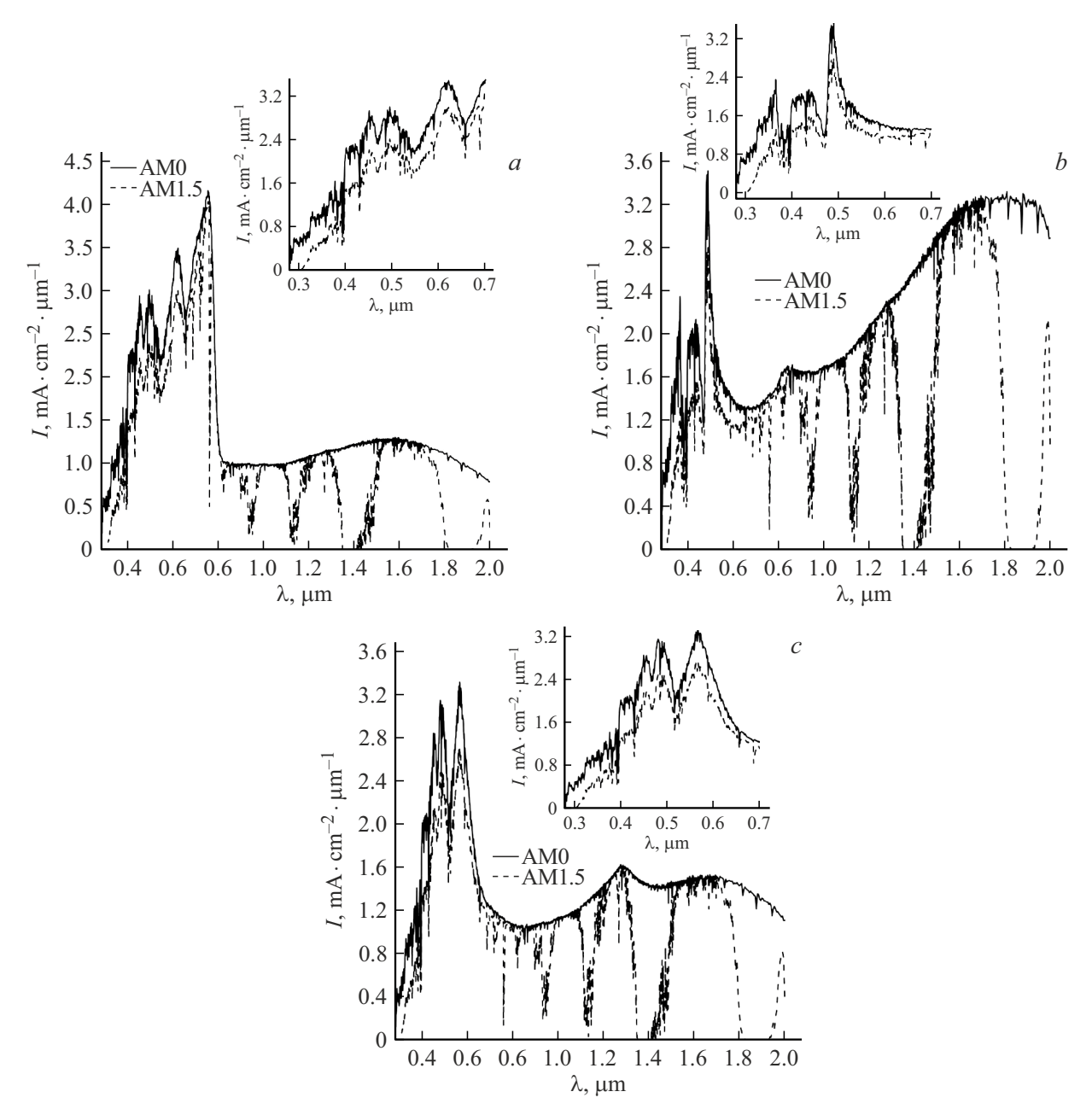


Figure 6. Photocurrent spectra on the Earth's surface (AM1.5) and outside the Earth's atmosphere (AM0) for borophene/GaN heterostructures: (a) without deformation; (b) in case of uniaxial compression by 14%; (c) in case of biaxial compression by 4%. The inserts to the figures show fragments of the photocurrent spectra in the wavelength range of $0.28 - 0.7 \,\mu\text{m}$.

ing deformation by 10,% leads to a twofold increase in the maximum integral photocurrent in the near-infrared range (wavelength of $1.2 \mu m$) while maintaining the maximum photocurrent in the visible radiation range (Fig. 7, b). The biaxial compression deformation by 6% causes an increase in the integral magnitude of the photocurrent over the entire considered range of infrared wavelengths and an almost twofold increase in the maximum photocurrent in the visible radiation range (Fig. 7, c). In general, it can be noted that the revealed patterns of changes in the absorption coefficient in the considered wavelength range for the

studied heterostructures in the presence of deformation are also manifested in the photocurrent spectra calculated on the basis of absorption spectra.

5. Conclusion

Thus, the use of an uniaxial and biaxial stretching and compression deformation makes it possible to control the optical (absorption coefficient) and optoelectronic (integrated magnitude of photocurrent) characteristics of van der Waals borophene/GaN and borophene/ZnO heterostructures

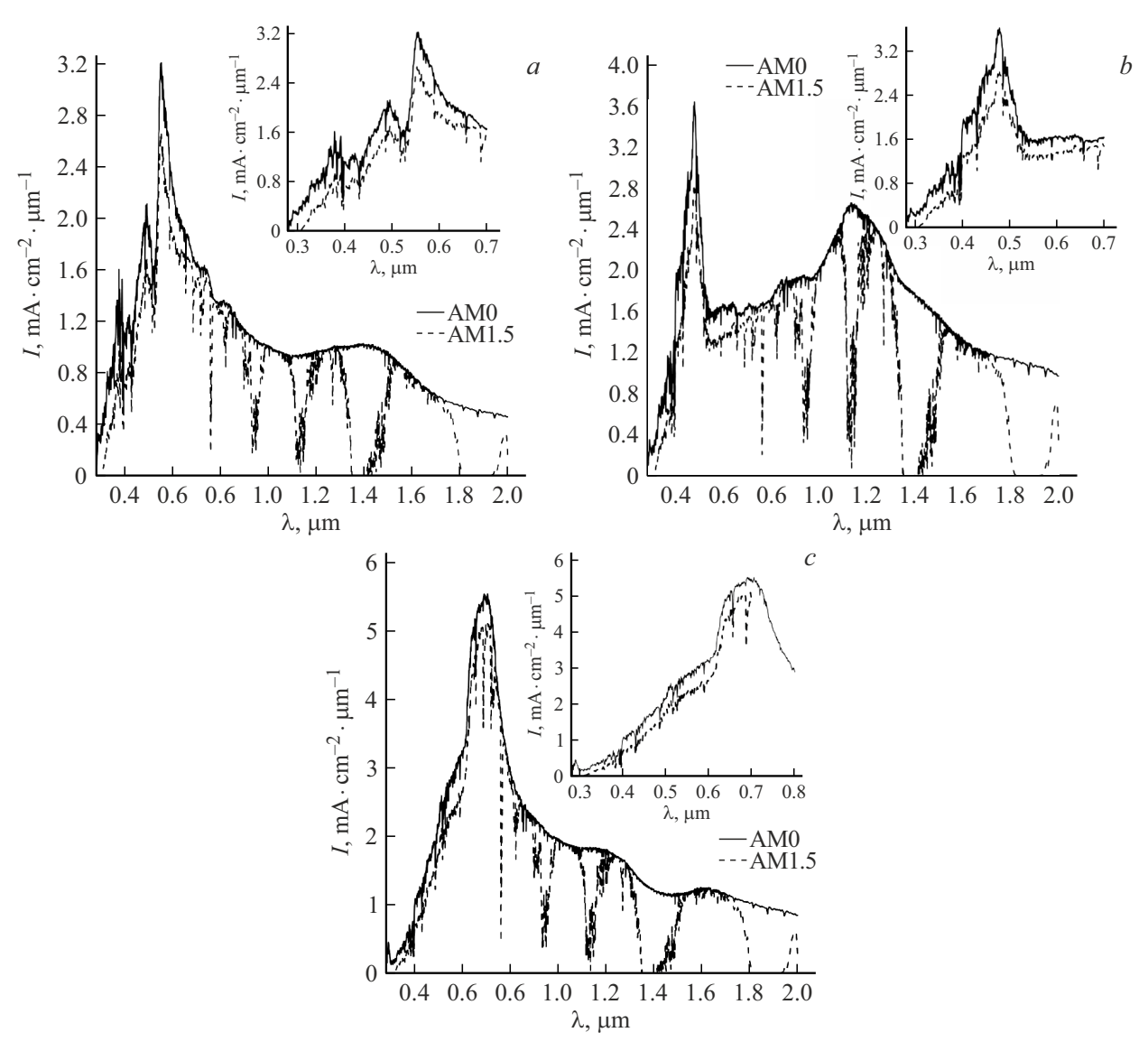


Figure 7. Photocurrent spectra on the Earth's surface (AM1.5) and outside the Earth's atmosphere (AM0) for borophene/ZnO heterostructures: (a) without deformation; (b) in case of uniaxial tension by 10%; (c) in case of biaxial compression by 6%. The inserts to the figures show fragments of the photocurrent spectra in the wavelength range of $0.28-0.7 \mu m$.

based on corrugated borophene with a triangular crystal lattice. The appearance of an energy gap between the valence band and the conduction band in the electronic structure of borophene heterostructures leads to an increase in the absorption coefficient and the integral magnitude of the photocurrent in the IR range, which is especially noticeable in the case of uniaxial compression deformation of the borophene/GaN heterostructure by 14%. In the direction of light polarization along the zigzag edge of the borophene sheet, the effect of uniaxial deformations on the quantitative changes in the absorption coefficient and, as a result, the integral magnitude of the photocurrent is more noticeable attributable to the fact that borophene atoms in this direction form zigzag chains with many cross-links that exert noticeable resistance to deformation. It is predicted

that the van der Waals heterostructures borophene/GaN and borophene/ZnO, in the presence of stretching and compression deformations leading to the appearance of an energy gap in their band structure, may be promising as sensitive elements of IR solar cells operating both on the Earth's surface and beyond, as well as in as effective IR radiation detectors.

Funding

The study was supported by a grant from the Russian Science Foundation (project No.21-72-00082, https://rscf.ru/project/21-72-00082 /) and the state assignment of the Ministry of Education and Science FSRR-2023-0008.

Conflict of interest

The authors declare that they have no conflict of interest.

References

- K.S. Novoselov, A.K. Geim, S.V. Morozov, D. Jiang, Y. Zhang, S.V. Dubonos, I.V. Grigorieva, A.A. Firsov. Science, 306 666 (2004). DOI: 10.1126/science.110289
- [2] P. Ares, K.S. Novoselov. Nano Mater. Sci., 4, 3 (2021). DOI: 10.1016/j.nanoms.2021.05.002
- [3] M. Corso, W. Auwarter, M. Muntwiler, A. Tamai, T. Greber, J. Osterwalder. Science, 303, 217 (2004). DOI: 10.1126/science.10919
- [4] L. Li, Y. Yu, G.J. Ye, Q. Ge, X. Ou, H. Wu, D. Feng, X.H. Chen, Y. Zhang. Nat. Nanotechnol., 9, 372 (2014). DOI: 10.1038/nnano.2014.35
- [5] L. Tao, E. Cinquanta, D. Chiappe, C. Grazianetti, M. Fanciulli, M. Dubey, A. Molle, D. Akinwande. Nat. Nanotechnol., 10, 227 (2015). DOI: 10.1038/nnano.2014.325
- [6] F.F. Zhu, W.J. Chen, Y. Xu, C.L. Gao, D.D. Guan, C.H. Liu, D. Qian, S.C. Zhang, J.F. Jia. Nat Mater., 14, 1020 (2015). DOI: 10.1038/nmat4384
- M. Davila, L. Xian, S. Cahangirov, A. Rubio, G. Le Lay. New J. Phys., 16, 095002 (2014).
 DOI: 10.1088/1367-2630/16/9/095002
- [8] S. Manzeli, D. Ovchinnikov, D. Pasquier, O.V. Yazyev, A. Kis. Nat. Rev. Mater., 2, 17033 (2017).DOI: 10.1038/natrevmats.2017.33
- [9] M.M. Uddin, M.H. Kabir, M.A. Ali, M.M. Hossain, M.U. Khandaker, S. Mandal, A. Arifutzzaman, D. Jana. RSC Adv., 13, 33336 (2023). DOI: 10.1039/d3ra04456d
- [10] Y.V. Kaneti, D.P. Benu, X. Xu, B. Yuliarto, Y. Yamauchi, D. Golberg. Chem. Rev., 122, 1000 (2021). DOI: 10.1021/acs.chemrev.1c00233
- [11] C. Hou, G. Tai, Z. Wu, J. Hao. Chempluschem., 85, 2186 (2020). DOI: 10.1002/cplu.202000550
- [12] K. Wang, S. Choyal, J.F. Schultz, J. McKenzie, L. Li, X. Liu,
 N. Jiang. Chempluschem., 89, e202400333 (2024).
 DOI: 10.1002/cplu.202400333
- [13] P. Ranjan, J.M. Lee, P. Kumar, A. Vinu. Adv. Mater., 32, 2000531 (2020). DOI: 10.1002/adma.202000531
- [14] G.H. Gupta, S. Kadakia, D. Agiwal, T. Kesharia, S. Kumar. Mater. Adv., 5, 1803 (2024). DOI: 10.1039/D3MA00829K
- [15] P. Kumar, G. Singh, R. Bahadur, Z. Li, X. Zhang, C.I. Sathish, M.R. Benzigar, T.K.A. Tran, N.T. Padmanabhan, S. Radhakrishnan, J.C. Janardhanan, C.A. Biji, A.J. Mathews, H. John, E. Tavakko, A. Vinu. Prog. Mater. Sci., 146, 101331 (2024). DOI: 10.1016/j.pmatsci.2024.101331
- [16] Z. Luo, X. Fan, Y. An. Nanoscale Res. Lett., 12, 514 (2017). DOI: 10.1186/s11671-017-2282-7
- [17] X.B. Li, S.Y. Xie, H. Zheng, W.Q. Tian, H.B. Sun. Nanoscale, 7, 18863 (2015). DOI: 10.1039/c5nr04359j
- [18] K.C. Lau, R. Pati, R. Pandey, A.C. Pineda. Chem. Phys. Lett.,
 418, 549 (2006).
 DOI: 10.1016/j.cplett.2005.10.104
- [19] X. Wu, J. Dai, Y. Zhao, Z. Zhuo, J. Yang, X.C. Zeng. ACS Nano, 6, 7443 (2012). DOI: 10.1021/nn302696v
- [20] D. Li, J. Gao, P. Cheng, J. He, Y. Yin, Y. Hu, L. Chen, Y. Cheng, J. Zhao. Adv. Funct. Mater., 30, 1904349 (2019). DOI: 10.1002/adfm.201904349

- [21] A. Horri, R. Faez. Micro Nano Lett., 14, 992 (2019). DOI: 10.1049/mnl.2019.0023
- [22] A.J. Mannix, X.-F. Zhou, B. Kiraly, J.D. Wood, D. Alducin, B.D. Myers, X. Liu, B.L. Fisher, U. Santiago, J.R. Guest, M.J. Yacaman, A. Ponce, A.R. Oganov, M.C. Hersam, N.P. Guisinger. Science, 350, 1513 (2015). DOI: 10.1126/science.aad1080
- [23] H. Sun, Q. Li, X.G. Wan. J. Am. Chem. Soc., 18, 14927 (2016). DOI: 10.1039/C6CP02029A
- [24] R. Yanga, M. Sun, J. Mater. Chem. C, 11, 6834 (2023). DOI: 10.1039/D3TC00974B
- [25] S. Wang, Q. Li, K. Hu, Q. Liu, X. Liu, X. Kong. Compos — A: Appl. Sci. Manuf., 138, 106033 (2020). DOI: 10.1016/j.compositesa.2020.106033
- [26] C. Hou, T. Ga, B. Liu, Z. Wu, Y. Yin. Nano Res., 14, 2337 (2021). DOI: 10.1007/s12274-020-3232-8
- [27] J. Yu, M. Zhou, M. Yang, Y. Zhang, B. Xu, X. Li, H. Tao. Adv. Mater. Interfaces, 9, 2102088 (2022). DOI: 10.1002/admi.202102088
- [28] J. Shen, Z. Yang, Y. Wang, L.C. Xu, R. Liu, X. Liu. Appl. Surf. Sci., 504, 144412 (2020). DOI: 10.1016/j.apsusc.2019.144412
- [29] C. Hou, G. Tai, Y. Liu, Z. Wu, Z. Wua, X. Liang. J. Mater. Chem. A, 9, 13100 (2021). DOI: 10.1039/D1TA01940F
- [30] J.W. Jiang, X.C. Wang, Y. Song, W.B. Mi. Appl. Surf. Sci., 440, 42 (2018). DOI: 10.1016/j.apsusc.2018.01.140
- [31] N. Katoch, A. Kumar, R. Sharma, P.K. Ahluwalia, J. Kumar. Phys. E: Low-Dimens. Syst. Nanostructures, 120, 113842 (2020). DOI: 10.1016/j.physe.2019.113842
- [32] S. Jing, W. Chen, J. Pan, W. Li, B. Bian, B. Liao, G. Wang. Mater. Sci. Semicond. Process., 146, 106673 (2022). DOI: 10.1016/j.mssp.2022.106673
- [33] M.M. Slepchenkov, D.A. Kolosov, O.E. Glukhova. Materials, 15, 4084 (2022). DOI: 10.3390/ma15124084
- [34] J.M. Soler, E. Artacho, J.D. Gale, A. García, J. Junquera, P. Ordejón, D. Sánchez-Portal. J. Phys.: Condens. Matt., 14, 2745 (2002). DOI: 10.1088/0953-8984/14/11/302
- [35] J.P. Perdew, J.A. Chevary, S.H. Vosko, K.A. Jackson, M.R. Pederson, D.J. Singh, C. Fiolhais. Phys. Rev. B, 46, 6671 (1992). DOI: 10.1103/PhysRevB.46.6671
- [36] S. Grimme. J. Comput. Chem., 27, 1787 (2006).DOI: 10.1002/jcc.20495
- [37] P. Pulay. Chem. Phys. Lett., 73, 393 (1980).DOI: 10.1016/0009-2614(80)80396-4
- [38] H.J. Monkhorst, J.D. Pack. Phys. Rev. B, 13, 5188 (1976). DOI: 10.1103/PhysRevB.13.5188
- [39] E.N. Economou. *Green's Functions in Quantum Physics*, 3rd ed. (Springer, Berlin, 1983), pp. 55–75.
 DOI: 10.1007/3-540-28841-4_4
- [40] M.M. Slepchenkov, D.A. Kolosov, O.E. Glukhova. Technical Physics, 69 (3), 397 (2024). DOI: 10.21883/0000000000.
- [41] M.M. Slepchenkov, D.A. Kolosov, O.E. Glukhova. Opt. Spectrosc., **131** (6), 712 (2023). DOI: 10.61011/EOS.2023.06.56658.115-23.
- [42] National Renewable Energy Laboratory (NREL) [electronic resource]. URL: https://www.nrel.gov/

Translated by A.Akhtyamov